Investigating profile stiffness and critical gradients in shaped TCV discharges using local gyrokinetic simulations of turbulent transport

G. Merlo[1], S. Brunner[1], O. Sauter[1], Y. Camenen[2], T. Görler[3], F. Jenko[3], A. Marinoni [4], D. Told[3] and L. Villard[1]

[1]Ecole Polytechnique Fédérale de Lausanne (EPFL), Centre de Recherches en Physique des Plasmas (CRPP), CH-1015 Lausanne, Switzerland
[2]Aix-Marseille Université CNRS, PIIM UMR 7345, 13397, Marseille, France
[3]Max-Planck-Institut für Plasmaphysik, Boltzmannstr. 2, D-85748 Garching, Germany
[4]Massachusetts Institute of Technology, Plasma Science and Fusion Center, Cambridge, MA 02139, USA

E-mail: gabriele.merlo@epfl.ch

Abstract. The experimental observation made on the TCV tokamak of a significant confinement improvement in plasmas with negative triangularity ($\delta < 0$) compared to those with standard positive triangularity has been interpreted in terms of different degrees of profile stiffness (Sauter *et al. Phys. Plasmas* **21** 055906, 2014) and/or different critical gradients. Employing the Eulerian gyrokinetic code GENE (Jenko *et al. Phys. Plasmas* **7** 1904, 2000), profile stiffness and critical gradients are studied under TCV relevant conditions. For the considered experimental discharges, trapped electron modes (TEMs) and electron temperature gradient (ETG) modes are the dominant microinstabilities, with the latter providing a significant contribution to the non-linear electron heat fluxes near the plasma edge. Two series of simulations with different levels of realism are performed, addressing the question of profile stiffness at various radial locations. Retaining finite collisionality, impurities and electromagnetic effects, as well as the physical electron-to-ion mass ratio are all necessary in order to approach the experimental flux measurements. However, flux-tube simulations are unable to fully reproduce the TCV results, pointing towards the need to carry out radially nonlocal (global) simulations, i.e. retaining finite machine size effects, in a future study. Some conclusions about the effect of triangularity can nevertheless be drawn based on the flux-tube results. In particular, the importance of considering the sensitivity to both temperature and density gradient is shown. The flux tube results show an increase of the critical gradients towards the edge, further enhanced when $\delta < 0$, and they also appear to indicate a reduction of profile stiffness towards plasma edge.

1. Introduction

Understanding and possibly reducing turbulent transport caused by microinstabilities is one of the key steps towards the success of any future fusion experiment, such as ITER

and DEMO. To this end, changing the shape of the Last Closed Flux Surface (LCFS) of the confined plasma is one of the known ways to directly influence the behaviour of the plasma down to the microscopic scales.

Of much interest along this line is the not yet fully understood experimental observation made on the TCV tokamak that in order to maintain the same electron temperature and density profiles, only half as much heating power is required for a discharge with negative triangularity $\delta_{\mathrm{LCFS}} = -0.4$ of the LCFS compared to a standard D-shape (positive $\delta_{\mathrm{LCFS}} = +0.4$) plasma [1]. This leads to an increase, by approximately a factor two, of the energy confinement, and is therefore an effect deserving further investigation. The physical mechanism leading to this improvement and in particular how triangularity, which has a finite penetration depth, can influence the behaviour of the plasma at all radial positions still remains unclear.

The gyrokinetic description of a plasma provides the appropriate framework for studying the effect of plasma shaping and understanding the origin of the observed confinement improvement. This topic has already been partly addressed in the past by Marinoni *et al.* [2]. In this study, a large number of non-linear flux-tube simulations carried out with the Eulerian, local, GS2 code [3] aimed at reproducing the measured heat transport reduction between the two plasma shapes. This study was able to recover a reduction of electron heat transport from negative triangularity, but only in the outermost region of the plasma where the triangularity is large. In the core plasma no sensible difference between positive and negative δ_{LCFS} plasmas was found, in agreement with the fact that triangularity has a finite penetration depth and tends to vanish at such radial locations.

A more recent observation, based on a large database of TCV discharges, showed that temperature and density profiles appear to be characterized over a wide range of plasma parameters by constant *logarithmic gradients* $R|\nabla \log(T, n)|$ in the core plasma, while constant *gradients* $|\nabla T, n|$, whose values vary with plasma parameters, characterizes the edge [4]. Here the core plasma is identified as the region between the sawtooth inversion radius and a radial location ρ_V of about 0.8, where $\rho_V = \sqrt{V/V_{\mathrm{LCFS}}}$ is the flux surface label based on the normalized plasma volume (V_{LCFS} is the volume enclosed by the plasma boundary). The edge region, on the other hand, is the outermost part of the plasma but still inside the LCFS, namely $0.8 \lesssim \rho_V < 1$. This observation is directly related to profile stiffness, i.e. the local slope of the flux versus normalized gradient curves, which thus appears to be strong and plasma parameters independent in the core and weaker and parameter dependent in the edge.

One can thus speculate that this radially varying stiffness, possibly together with varying values of the non-linear critical gradients $R/L_{T_{e,crit}}$ for instability, can be related to the beneficial effect of negative δ. Two limiting cases of such a relation are depicted in the two cartoons of figure 1. A first possibility, shown in cartoon (a), is that the level of edge stiffness is triangularity-dependent and is reduced going from positive to negative $\delta_{\mathrm{LCFS}} < 0$, while $R/L_{T_{e,crit}}$ does not depend on triangularity. The second limiting case is that the degree of edge non-stiffness is not related to δ, however the critical gradient

$R/L_{T_{e,crit}}$ depends on shape and is larger for plasmas with negative triangularity. This second case is depicted in cartoon (b) of figure 1. In both these limiting cases, or any combination in between, the confinement improvement would rely entirely on the edge region where the triangularity is indeed strong. In both cases, a stiff core profile leading to the same logarithmic gradient even when the heat flux varies by a factor of 2, explains the transport behaviour in this inner region.

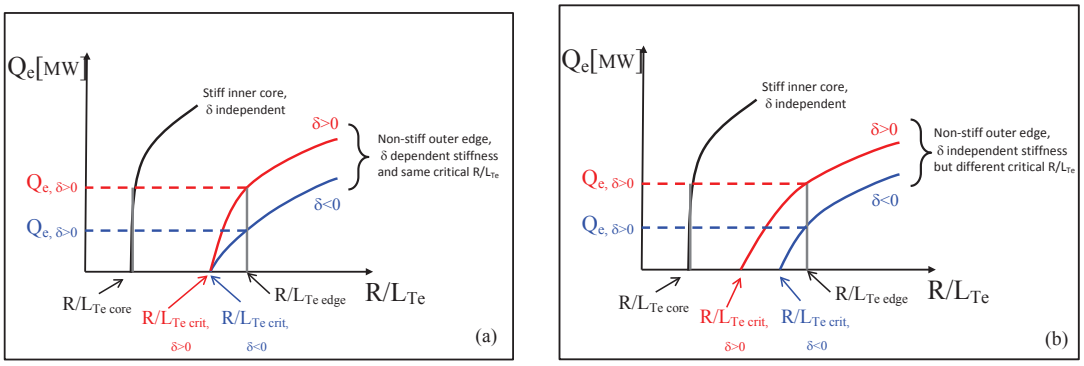

Figure 1. Cartoons describing two limiting ways of relating the confinement improvement associated with negative triangularity to profile stiffness. (a) via enhanced edge non-stiffness when $\delta_{\mathrm{LCFS}} < 0$ but same critical gradients, and (b) higher $R/L_{T_{e,crit}}$ at the same edge non-stiffness.

The goal of this work is therefore to study profile stiffness in conditions relevant to the TCV tokamak, with the final objective of verifying the hypotheses of a radially varying and triangularity-dependent stiffness. At the same time, the dependence of critical gradients $R/L_{T,n_{,crit}}$ on δ can be addressed. Flux tube simulations are the natural tool to be used for such a study, as they allow to easily vary the local electron temperature and density gradients $R/L_{T_e,n_e}$ and compute the associated turbulent heat fluxes. Global simulations are computationally more expensive, and the interpretation of the results in terms of local stiffness might be not obvious. A first attempt to study profile stiffness with global simulations is presented in Ref. [5], where for a given TCV plasma shape the relation between increased heating and profiles evolution was studied in the ITG regime, obtaining a qualitative agreement with the experimental findings present in Ref. [4].

This paper is thus complementary to what was already published in Ref. [2], where the issue of profile stiffness was not addressed and it is also a further step towards aiming at quantitatively reproducing experimental measurements with gyrokinetic modeling. In order to carry out this study, we make systematic use of the gyrokinetic Eulerian code GENE [6]. First simulations results contained in this paper have already been published in Ref. [4] where the role of profile stiffness on transport in TCV discharges was addressed for the first time. We will present these results here in more detail as well as new ones considering a more accurate and realistic model. Considering finite collisionality, impurities and electromagnetic effects is necessary as all these effects

strongly influence turbulent transport leading to an overall flux reduction. It will nevertheless be shown that the local flux-tube simulations are unable to quantitatively reproduce the experimentally measured heat transport levels and therefore a definitive conclusion on profile stiffness cannot be drawn. Indeed, the electron heat flux predicted by the flux-tube simulations remains too large in comparison to the experimental results even considering the most accurate local modeling available, and the overestimation is particularly strong in the plasma core. It is thus concluded that finite machine size effects, the so-called finite ρ^* effects, $\rho^* = \rho_s/a$ (ρ_s being the ion sound Larmor radius and a the minor radius of the tokamak) are expected to be strong especially in smaller systems of the size of TCV for which $\rho^* = 1/80$ and radially nonlocal simulations would be required for reproducing the actual measurements.

The remainder of this paper is organized as follows: in section 2 the essential features of negative triangularity plasmas, and the relative confinement improvement, will be recalled. Section 3 contains the details of the simulation model. The results of linear simulations are presented in section 4 while the results from non-linear simulations are then presented in section 5. Finally, conclusions are drawn in section 6.

2. Reversing LCFS triangularity in the TCV tokamak

The TCV tokamak [7] (major radius R=0.88 m, minor radius at midplane a=0.25 m, magnetic field on axis B_0=1.44 T and plasma current I_p up to 1.0 MA) offers a unique plasma shaping capability. Indeed, discharges with an edge elongation κ up to 2.8 and triangularity $-0.7 \leq \delta_{\mathrm{LCFS}} \leq 1$ have been obtained. The effect of negative δ in L-mode discharges has been investigated with a dedicated triangularity scan in EC-heated plasmas with δ_{LCFS} ranging from -0.4 to 0.4. The interested readers are referred to [1, 8] for a detailed description of the experimental set-up. Let us recall here that in those discharges a specific effort was made in order to keep all other plasma parameters, and especially elongation [9], constant in order to highlight the effect of triangularity. The electron heat transport was experimentally determined by a power balance analysis. We note that the experimental error bars lead to an uncertainty of $\sim 20\%$ in the determination of the electron temperature and density gradients. This uncertainty is particularly important towards the plasma edge where the error bars in the extrapolation of the ion temperature profiles can reach up to 80-100%. Furthermore, at these radial locations the radiated power can represent a non-negligible fraction of the total electron heat flux (20-30%). The main result was that the same electron temperature and density profiles were achieved in plasmas with $\delta_{\mathrm{LCFS}} = +0.4$ and -0.4 but injecting in the latter case half as much heating power compared to the former. This was interpreted as a better energy confinement at all plasma radii, by a factor of two, when flipping the sign of δ_{LCFS}.

We will focus our attention on the discharges #28014 ($\delta_{\mathrm{LCFS}} = 0.4$) and #28008 ($\delta_{\mathrm{LCFS}} = -0.4$), for which the same profiles have been obtained with the injection of respectively 1.3 MW and 0.65 MW. The radial profiles of electron temperature

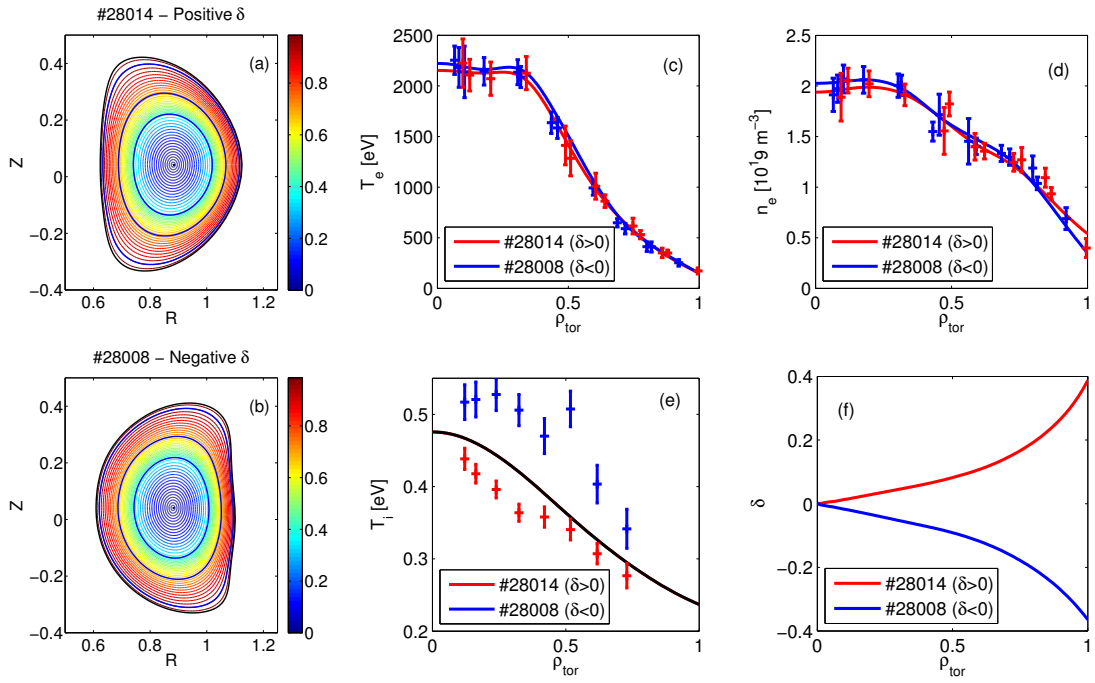

Figure 2. (Color online) TCV discharges #28014 and #28008 with resp. positive ($\delta_{\rm LCFS} = +0.4$) and negative ($\delta_{\rm LCFS} = -0.4$) triangularity of the LCFS. Corresponding flux surface contours of constant normalized poloidal flux $\Psi/\Psi_{\rm LCFS}$ are shown in (a) and (b) (blue curves indicate the the radial positions $\rho_{tor} = 0.5$, 0.7 and 0.95 where flux-tube simulations have been performed). Shown as a function of ρ_{tor} are the experimentally measured profiles of (c) electron temperature T_e and (d) electron density n_e as well as (e) the ion temperature T_i profile used for the simulations and (f) the triangularity δ as obtained from MHD equilibrium reconstructed with CHEASE.

T_e, electron density n_e and ion temperature T_i, together with the radial profile of triangularity, are shown in figure 2. We note that the experimentally measured ion temperature profiles are available only in the core plasma region and between the two discharges they are up to $\sim 40\%$ different, T_i being higher in the negative δ plasma. All the simulations presented here have been carried out considering an intermediate profile, depicted in black in figure 2.e, as already done in Ref. [2]. We have verified with linear simulations that this choice is not affecting the results, as only a maximum $\sim 3\%$ variation of the linear growth rates is found when changing the T_i profile between the experimental values.

3. Simulation details

The gyrokinetic simulations shown here have been carried out using the local (flux-tube) version of the GENE code [6]. GENE is an Eulerian code, i.e. the distribution functions of the different plasma species are discretized on a fixed grid in phase space. Linear and non-linear simulations of microturbulence can be carried out, considering fully kinetic multi-species dynamics, for which electrostatic and electromagnetic fluctuations can be

considered. Intra- and inter-species collisions (both pitch angle and energy scattering) are implemented, while interfaces to MHD equilibrium codes such as CHEASE [10] are available.

GENE adopts a field aligned coordinate system (x, y, z) to discretize the configuration space, while $(v_\parallel, \mu)$ are used as velocity variables. Here x stands for the radial, y for the binormal and z is the straight-field line poloidal angle parametrizing the position along a given field line, and therefore is referred to as "parallel" direction. The variable $\mu = mv_\perp/2B$ represents the magnetic moment, while $v_\parallel$ and $v_\perp$ the components of velocity respectively parallel and perpendicular to the magnetic field; m is the mass of the particle and B the local magnitude of the magnetic equilibrium field $\mathbf{B}$. In the flux-tube version of the code, Fourier representation is used for the x and y directions. To ensure numerical convergence of each simulation, different box sizes $L_x \times L_y$ have been used together with different phase space resolutions, as reported in tables 2 and 3. The limits for the velocity space grids of each $j-$species were set from -3 to 3 for $v_\parallel/v_{th,j}$ and from 0 to 9 for $\mu B_0/T_j$, $v_{th,j} = \sqrt{2T_j/m_j}$ being the thermal velocity and B_0 the magnetic field on axis.

In order to model conditions relevant for studying stiffness and the confinement improvement associated to negative δ plasma, the two TCV discharges #28014 and #28008 described in section 2 are considered. Three different radial positions $\rho_{tor} = 0.5$, 0.7 and 0.95 have been considered for both discharges. They are representative of core, intermediate and edge conditions. Here ρ_{tor} is the radial coordinate based on the toroidal flux Φ, $\rho_{tor} = \sqrt{\Phi/\Phi_{\rm LCFS}}$. The magnetic equilibrium reconstructed with CHEASE has been used. The physical parameters describing the two discharges at the three considered radii, and used for the simulations, are listed in table 1. Temperature and density gradient lengths are defined according to the following relation:

$$R/L_{T,n} = -R/\alpha/d\log(T,n)/d\rho_{tor}. \tag{1}$$

with $\alpha = \sqrt{(\Phi_{\rm LCFS}/piB_0)}$. The plasmas are Deuterium discharges. The effective charge, defined as $Z_{\rm eff} = \sum_i n_i Z_i^2/\sum_i n_i$ where the sums are over all ion species, takes on the value $Z_{\rm eff} \approx 3.6$, with carbon ($Z_C = 6$) the dominant impurity. Three fully kinetic species have thus been considered in the GENE simulations: Deuterium ions, electrons and Carbon ions. Deuterium and carbon concentrations are estimated so as to respect quasineutrality, i.e. $n_D + Z_C n_C = n_e$ and in agreement with the experimentally measured value of $Z_{\rm eff}$. As $Z_{\rm eff}$ is assumed to be radially constant, one has $R/L_n = R/L_{n_e} = R/L_{n_D} = R/L_{n_C}$. When considering electromagnetic effects, the experimental value of $\beta_e = 2\mu_0 p_e/B_0^2$ is used; p_e is the local electron pressure. For the simulations in which finite collisionality is accounted for, it is evaluated based on the experimental values. In particular, $\nu_{ei} = \sum_i 3\sqrt{\pi}/4\tau_{e,i}$, where $\tau_{e,i}$ is the electron collision time of the i-th ion species, $\tau_{e,i} = 3(2\pi)^{3/2}\epsilon_0^2 T_e^{3/2} m_e^{1/2}/n_i Z_i^2 e^2 \log\Lambda$, m_e is the electron mass and $\log\Lambda$ is the Coulomb logarithm. In order to conform to the experimental observation that within error bars the temperature and density profiles are the same, we used in all simulations, for both positive and negative δ, the measurements associated

to the positive δ discharge, but keeping the relevant equilibrium depending on $\delta_{\rm LCFS}$.

	ρ_{tor}=0.5	ρ_{tor}=0.7	ρ_{tor}=0.95
q	1.18(1.26)	1.81(1.92)	3.58(3.66)
$\hat{s}$	0.82(0.78)	1.73(1.67)	3.31(2.53)
δ	0.09(-0.09)	0.15(-0.15)	0.33(-0.31)
T_i/T_e	**0.252**(0.289)	**0.43**(0.47)	**1.13**(1.11)
R/L_n	**3.75**(2.99)	**3.61**(4.39)	**10.4**(19.2)
R/L_{T_e}	**8.99**(8.89)	**10.52**(12.56)	**17.2**(18.8)
R/L_{T_i}	2.59	2.49	1.8
$\nu_{ei}[c_s/R]$	0.32(0.30)	1.12(1.02)	5.18(4.07)
β_e	0.41(0.44) $\times 10^{-2}$	0.16(0.16) $\times 10^{-2}$	0.26(0.21) $\times 10^{-3}$

Table 1. Experimental parameters describing the three radial positions considered for flux-tube simulations. q = safety factor, $\hat{s}$ shear and other parameters defined in main text. Listed are the values referring to the TCV discharge #28014, positive δ, while the corresponding values for negative δ are provided in parenthesis. The values related to temperature and density profiles used for both $\delta > 0$ and $\delta < 0$ simulations are highlighted in bold.

4. Linear simulations

The GENE code has first been used in its linear version in order to identify for both considered triangularities the most unstable eigenmodes for the three radial positions ρ_{tor}=0.5, 0.7 and 0.95. Wavenumbers $k_y\rho_s$ up to the electron scale have been considered. The growth rate γ and the real frequency ω_r, normalized to R/c_s, are shown as a function of $k_y\rho_s$ in figure 3. The results are shown in figures figs. 3.a), c) and e) in log-log plots over both ions and electron scales. To emphasize the difference between the results at the ion scale obtained with the two triangularities, the corresponding growth rates are also shown in lin-lin plots in figs. 3.b), d) and f). Here $c_s = \sqrt{T_e/m_i}$ is the ion sound speed and ρ_s the ion sound Larmor radius $\rho_s = c_s/\Omega_i$ where $\Omega_i = eB_0/m_i$ is the ion cyclotron frequency. Note that the normalization factors are all based on the local value of the sound speed. The mode real frequency is depicted with a dashed line, and for all the wavenumbers considered it has a negative sign, indicating, in agreement with to GENE conventions, that the mode propagates in the electron diamagnetic direction. According to the GENE definition of the y variable, each k_y can be associated to a given toroidal mode number $n = k_y\rho_{tor}/q$, where ρ_{tor} is the radial position at which the flux tube is centered. The k_y associated to the $n = 1$ mode can be thus considered as the smallest physical wavenumber. These simulations have been performed considering a $n_{k_x} \times n_z \times n_{v_\parallel} \times n_\mu$= 64 $\times$ 64 $\times$ 64 $\times$ 16 grid, enough to ensure the convergence of the results within 10%. Electromagnetic fluctuations (without $B_\parallel$ contribution), finite collisionality and the experimentally measured Carbon content have all been retained.

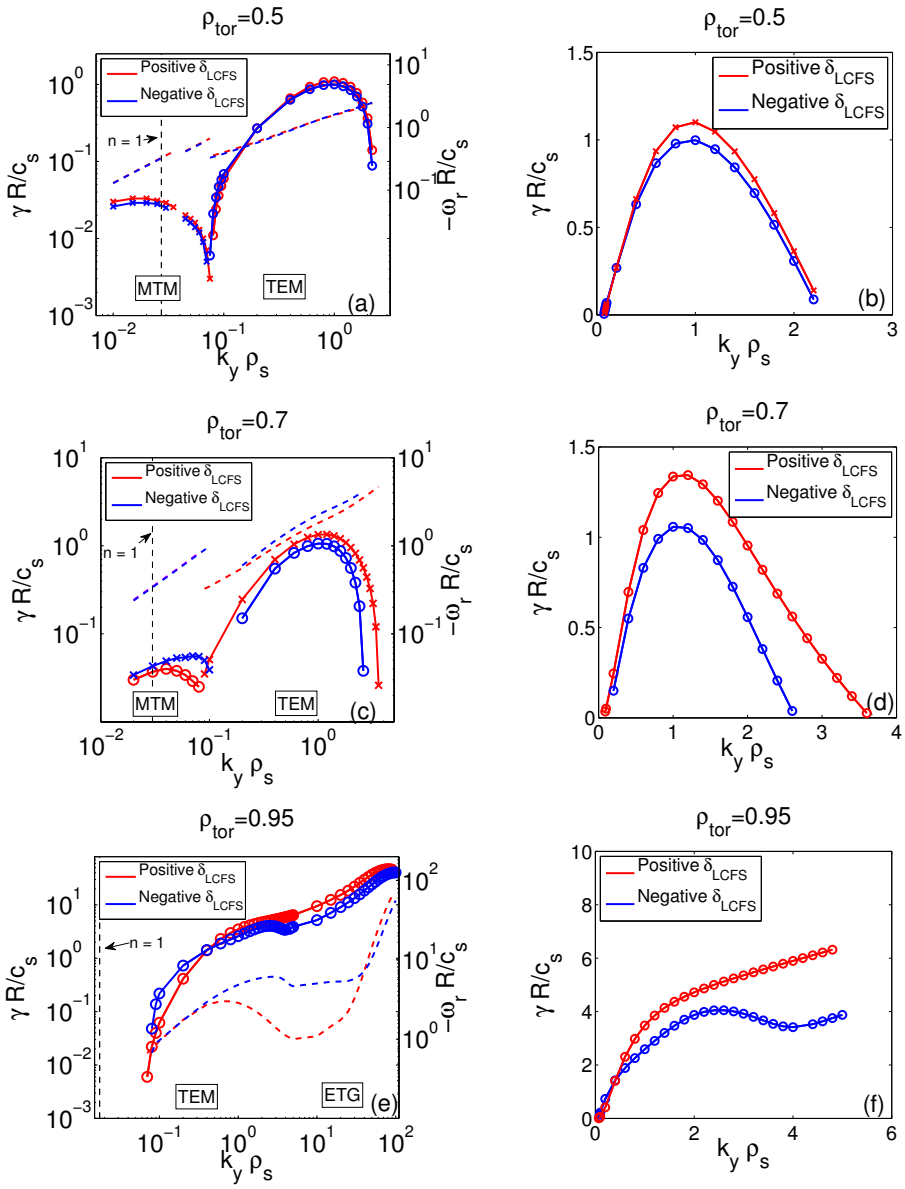

Figure 3. Linear growth rates (continuous lines) and real frequency (dashed lines) in units of c_s/R as a function of the wavenumber $k_y\rho_s$ for (a, b) ρ_{tor}=0.5, (c, d) ρ_{tor}=0.7 and (e, f) ρ_{tor}=0.95. (a), (c) and (e) plots in log-log scale, (b) and (d) and $f)$ in lin-lin scale limited to the ion scale. Frequency ω_r are shown only in log-log plots. Shown are the results obtained for TCV discharges #28014 (red) and #28008 (blue). All modes propagate in the electron diamagnetic direction; MTM instabilities are marked with a cross while TEM/ETG with circles. Vertical dashed lines indicate the approximate wavenumber corresponding to the n=1 toroidal mode number.

These physical effects correspond to the "*full physics*" model set-up used for non-linear simulations and presented in section 5.

At all the considered positions, for both positive and negative δ, trapped electron modes (TEMs) are the most unstable instability at the ion scale. The negative triangularity discharge is found to have lower growth rates than the one with positive

$\delta_{\rm LCFS}$ at all $k_y\rho_s$ scales, with the exception of the $\rho_{tor} = 0.95$ position where for $k_y \lesssim 0.2$ the behaviour is inverted. For essentially all $k_y\rho_s$, the difference between the growth rates for the two triangularity cases increases as one moves towards the plasma edge, i.e. when positive respectively negative triangularity gets larger. This result is in agreement with the similar study reported in Ref. [2], where different radial locations were also considered.

At large scales ($k_y\rho_s < 0.1$), for the two innermost positions $\rho_{tor} = 0.5$ and $\rho_{tor} = 0.7$ microtearing modes (MTMs) [12] are the most unstable. The nature of these modes is determined by inspecting the parity of the ϕ and $A_\parallel$ fields with respect to the radial position of the mode rational surfaces. The growth rate is nevertheless small compared to TEM ones and it turns out that their contribution to the non-linear turbulent heat flux, which is essentially electrostatic, is negligible. At ρ_{tor}=0.95, MTMs are still unstable, but with a smaller growth rate compared to TEMs. Varying the electron temperature gradient at this location, one finds a transition from TEMs to MTMs for a gradient smaller than the experimental one, as can be seen in figure 4*c*).

We also studied instabilities at the electron scale. Electron temperature gradient (ETG) modes are destabilized only at $\rho_{tor} = 0.95$ by the strong gradients characteristic of this location [13]. For the other considered radii, the low T_i and large $Z_{\rm eff}$ are stabilizing to ETG modes. Despite the fact that for both positive and negative δ the TEM branch continuously evolves to the ETG one when going from ion ($k_y\rho_s \lesssim 1$) to electron scales ($k_y\rho_s \gg 1$), a stronger hump at the ion scale is found in the $\delta < 0$ case, reflecting a different interplay between the two scales according to the plasma shape considered.

Determining a linear critical gradient is a difficult exercise for the two discharges being considered here. For all cases, we have performed a scan of both electron temperature and density gradient for $k_y\rho_s = 0.3$ (the mode at which we expect the largest contribution to non-linear fluxes, ρ_s being the local value of the Larmor radius). The results are shown in figure 4, where the same aspect scale has been used when plotting the results relative to a given position (figures 4 $(a-d)$, $(b-e)$ and $(c-f)$) in order to allow the comparison of the sensitivity of the linear growth rates to a variation of temperature and density gradient. Almost no difference between the two shapes is found for the innermost core position where there is no critical temperature gradient, the TEMs being driven by both density and temperature gradients, while we find essentially the same critical density gradient length for the TEM ($R/L_n \simeq 1$). At $\rho_{tor} = 0.7$, no critical gradient is found for TEM when scanning the electron temperature gradient (for both shapes different TEMs branches exist at different value of $k_y\rho_s$ as shown in fig. 4.*b*), while scanning the density gradient one finds a linear critical gradient for TEMs at $R/L_n \simeq 1$ (resp. $R/L_n \simeq 2$) for positive (resp. negative) triangularity. Finally, at $\rho_{tor} = 0.95$ the difference between the two plasma shapes is most evident. For both positive and negative triangularity, no critical density gradient is found and at all R/L_n the growth rate of the most unstable mode for the negative triangularity shape turns out to be for the considered $k_y\rho_s$ bigger than the corresponding one for

positive triangularity. When scanning R/L_{T_e} we find that for the experimental value of the gradients, the positive $\delta_{\rm LCFS}$ discharge is more stable than the negative one, but as one further reduces R/L_{T_e} the $\delta_{\rm LCFS} < 0$ one returns to be more stable. We note that these orderings of the growth rates for the two triangularities are specific to the particular $k_y\rho_s$ that we considered. If one repeats the same exercise of varying the gradients but at different k_y (e.g. the one at which the linear growth rate is maximum), the results will look different. Especially, increasing k_y, we find that growth rates of TEMs become relatively larger and the negative δ discharge has lower growth rates at all positions and all temperature and density gradients. The results obtained scanning both temperature and gradient lengths are summarized for all the considered radial locations in figure 5, from which it appears clear how the maximum linear growth rate is more sensitive to a variation of the density gradient with respect to a variation of the temperature one. This difference is reduced moving from the core (ρ_{tor}=0.5) to the edge (ρ_{tor}=0.95), where independently from plasma triangularity a given variation of temperature or density gradient appears to induce the same change of the growth rate.

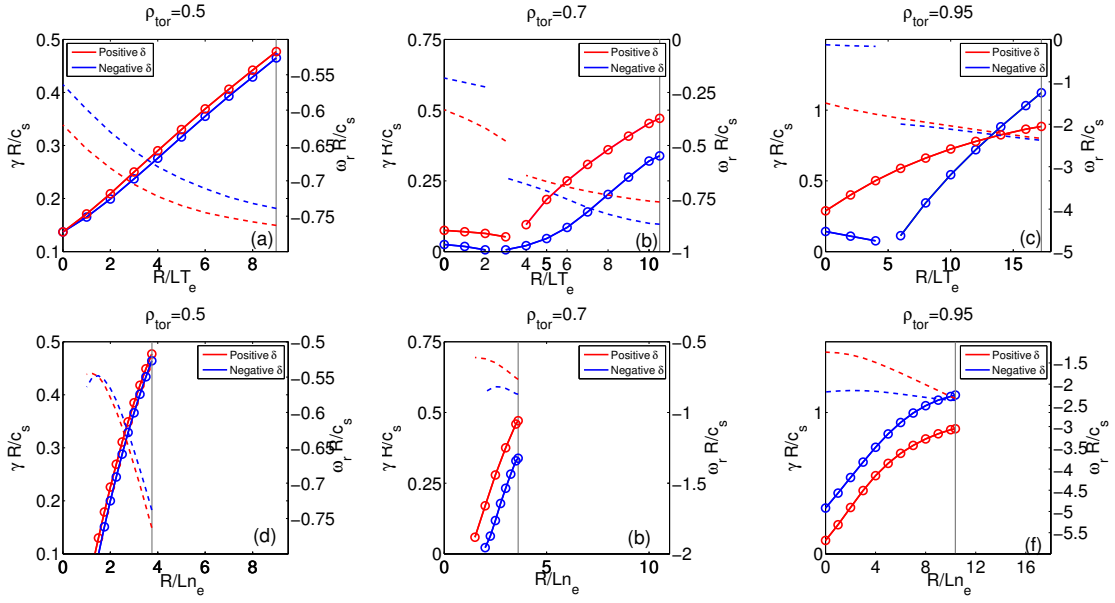

Figure 4. (Color online) Linear growth rates γ (continuous lines) and real frequency ω_r (dashed lines) of the $k_y\rho_s = 0.3$ mode in units of c_s/R as a function of (a, b, c) electron temperature gradient R/L_{T_e} and (d, e, f) density gradient R/L_{n_e}. Shown are the results for positive (red) and negative triangularity (blue) evaluated at (a, d) ρ_{tor}=0.5, (b, e) ρ_{tor}=0.7, and (c, f) ρ_{tor}=0.95. Vertical lines indicate the experimentally measured gradient.

5. Non-linear simulations

Non-linear simulations have been performed for the two TCV discharges at the three aforementioned radial locations. Two different simulation models have been considered.

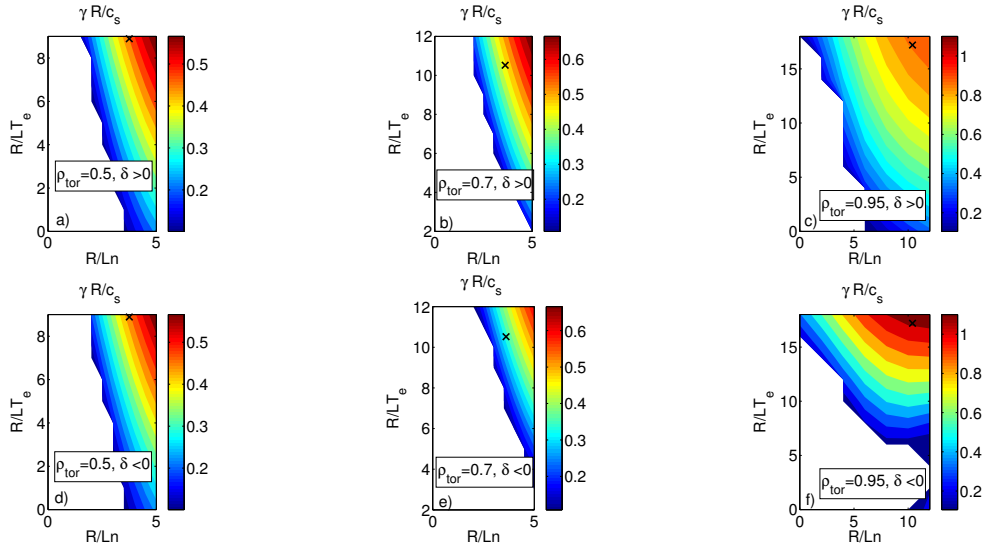

Figure 5. (Color online) Linear growth rates γ of the $k_y\rho_s = 0.3$ mode in units of c_s/R as a function of temperature and density gradient lengths. Shown are the results obtained for (a, b, c) positive δ plasma at respectively ρ_{tor}=0.5, 0.7 and 0.95, and (e, d, f) negative δ at the same radial location. The experimentally measured gradients are reported for each position with a black cross.

	L_x/ρ_s, $\delta > 0$	L_x/ρ_s, $\delta < 0$	L_y/ρ_s	$k_{x,\max}\rho_s$, $\delta > 0$	$k_{x,\max}\rho_s$, $\delta < 0$
ρ_{tor}=0.5	145(145)	153(153)	126(126)	2.76(5.52)	2.62(5.25)
ρ_{tor}=0.7	139(151)	143(155)	126(126)	4.33(5.33)	4.20(5.18)
ρ_{tor}=0.95	115(115)	120(120)	126(126)	10.52(10.52)	10.17(10.17)

Table 2. Flux-tube dimensions adopted for non-linear simulations. Listed are the values for the *"simple physics"* runs, while in parenthesis for the *"full physics"*. Lengths are normalized to the local sound larmor radius ρ_s. $k_{x,\max}\rho_s$ indicates the maximum radial wave vector retained in the simulation.

	n_{k_x}	n_{k_y}	n_z	$n_{v_\parallel}$	n_μ
ρ_{tor}=0.5	128(256)	64(64)	32(32)	48(64)	8(16)
ρ_{tor}=0.7	192(256)	64(64)	32(32)	48(64)	8(16)
ρ_{tor}=0.95	384(384)	64(64)	32(32)	48(64)	8(16)

Table 3. Resolutions adopted for non-linear simulations. Listed are the values for the *"simple physics"* runs, while in parenthesis for the *"full physics"*.

The first one, referred to in the following as "*simple physics*" model, considers only deuterium and electrons, the latter with an reduced ion-to-electron mass ratio (m_D/m_e=400). Furthermore, impurities, finite collisionality and electromagnetic effects have all been neglected. These approximations are made in order to reduce the cost of the runs, allowing more extensive parameter scans. As will be shown, this simple model has its limitations and all of above mentioned neglected effects have therefore been retained in a second series of simulations. These runs, referred to as "*full physics*"

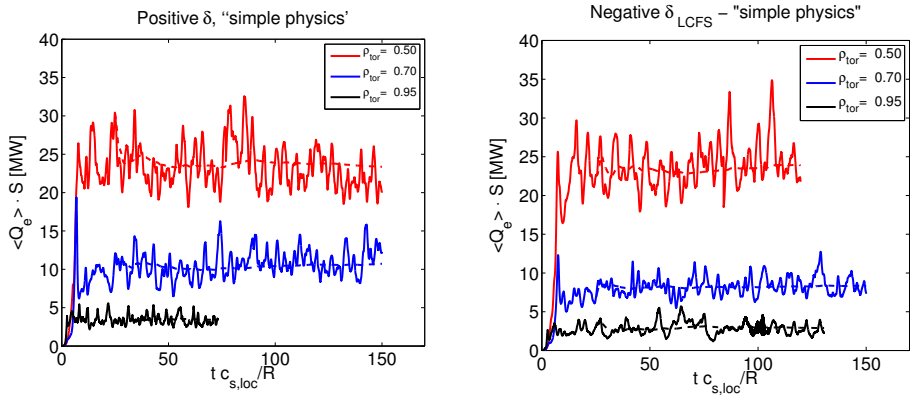

Figure 6. Time traces of the simulated electron heat power $\langle Q_e \rangle \cdot S$ in MW for (a) positive $\delta_{\rm LCFS}$ and (b) negative $\delta_{\rm LCFS}$ discharges. Shown are the results obtained for the radial positions $\rho_{tor} = 0.5$ (red), 0.7 (blue) and 0.95 (black). These simulations have been performed with the *"simple physics"* model. Dashed lines indicate the running averages. (Color online)

model, are fully-kinetic, electromagnetic, collisional runs, with the realistic electron mass and the experimental content of Carbon accounted for.

All the simulations have been limited to the ion gyroradius scale; numerical fourth order hyperdiffusion [14] is used to avoid spectral pile-ups due to medium k_y ETGs. The grid resolution used for these runs are reported in table 3. Higher radial resolutions are required for flux-tube simulations with radial position towards the plasma edge in conjunction with the increase of magnetic shear $\hat{s}$, see table 1 leading to a coupling of k_x modes that are further apart in k-space than at low shear [15]. At the same time, to limit the cost of these runs, the radial extent L_x of the box has been reduced in comparison with the more inner radial positions. Finally, retaining collisions requires a higher resolution in velocity space, explaining the different set-up of *"full physics"* runs.

5.1. "Simple physics" model

The time traces of the simulated electron heat power $\langle Q_e \rangle \cdot S$ in MegaWatts are shown in figure 6. The heat flux density $\langle Q_e \rangle$ is defined as the average over the flux-tube volume, $\langle Q_e \rangle = \int \mathbf{Q} \cdot \nabla x \; J^{xyz} \; dxdydz \Big/ L_x L_y \int |\nabla x| \; J^{xyz} \; dz$, J^{xyz} being the Jacobian of the (x, y, z) coordinate system, while S is the area of the flux surface of interest. $\mathbf{Q}$ is the (electron) heat flux, defined as $\mathbf{Q} = \int (1/2 m v^2 f v_{\mathbf{E}\times\mathbf{B}}) d^3v$, where f is the fluctuating part of the distribution function and $v_{\mathbf{E}\times\mathbf{B}}$ the generalized $\mathbf{E} \times \mathbf{B}$ velocity. The ion heat flux is negligible, and therefore not shown, in agreement with the fact that TEMs are the dominant instabilities. Note that each simulation time is normalized using the local values of the sound speed $c_{s,loc}$. Given the fact that the simulations at $\rho_{tor} = 0.95$ are significantly more expensive than the ones at the other positions, somewhat less statistics have been acquired for these outer radial runs. The corresponding turbulent k_y-spectra are shown in figure 7, where for each radial position the results from the two

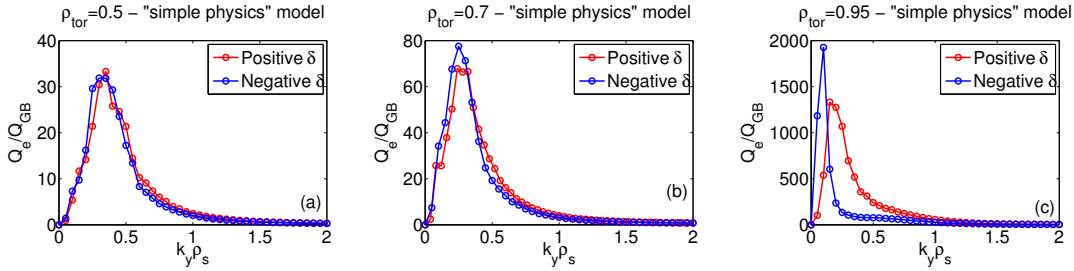

Figure 7. Electron heat flux spectra evaluated at (a) $\rho_{tor} = 0.5$, (b) $\rho_{tor} = 0.7$ and (c) $\rho_{tor} = 0.95$. The heat fluxes are normalized to the local value of $Q_{\rm GB} = c_s T_e n_e (\rho_s/R)^2$. Experimental temperature gradients considered.

shapes are compared. A reduction of the integrated fluxes is found when flipping δ sign for larger ρ_{tor} (Fig. 6 and in agreement with [2]). However there is not a systematic reduction of the contribution to the fluxes from a given k_y, as seen in Fig. 7. We also note that the value of k_y which contributes most to the transport is reduced as one moves towards the LCFS, independently from triangularity. At $\rho_{tor} = 0.95$ the difference between the two discharges appears strongest.

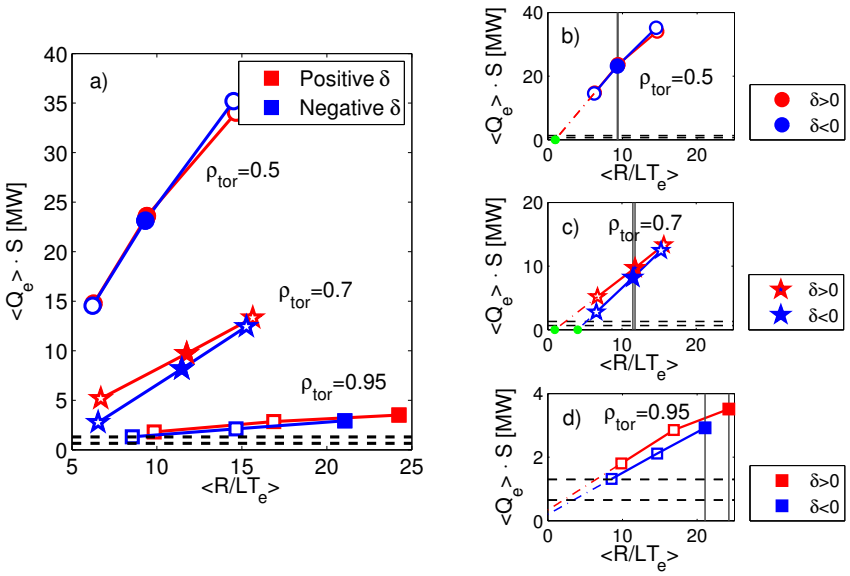

Figure 8. (Color online) Electron heat power in MW versus the flux surface-averaged logarithmic temperature gradient $\langle R/L_{T_e} \rangle$ obtained with "*simple physics*" model. Shown are the results obtained for positive (red) and negative δ (blue) at $\rho_{tor} = 0.5$ (circles), $\rho_{tor} = 0.7$ (stars) and $\rho_{tor} = 0.95$ (squares) . Full markers correspond to the experimental value of the gradient (further pointed out also with vertical lines), while horizontal lines indicate the input heating power for both positive and negative δ (1.3 MW and 0.65 MW respectively). For the sake of clearness, the same results are shown separately for each radial position, (a) $\rho_{tor} = 0.5$, (b) $\rho_{tor} = 0.7$ and (c) $\rho_{tor} = 0.95$. Linearly extrapolated critical gradients have been highlighted with dashed lines and green dots.

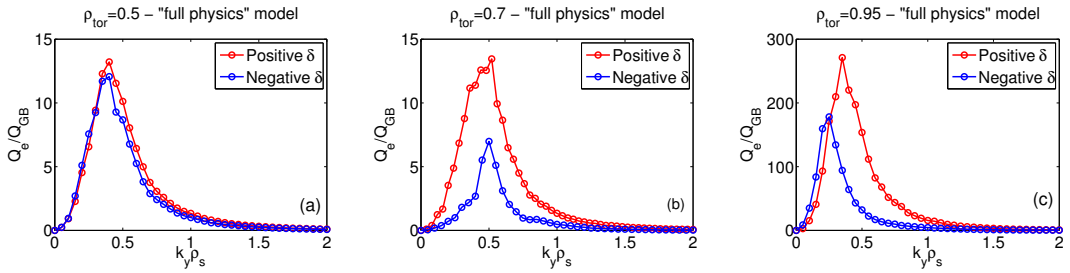

Figure 9. Same as figure 7 but for the "*full physics*" model results.

For each position, the electron temperature gradient was both reduced and increased from the experimental value in order to address stiffness. The results are shown in figure 8. In this plot, and in all the following figures, the same color coding is used to help the reader. Red curves (color online) refer to the shape with positive triangularity, blue ones to the negative. Circles are used to mark $\rho_{tor} = 0.5$ position, stars $\rho_{tor} = 0.7$ and squares $\rho_{tor} = 0.95$. Finally, full-colored markers indicate the experimental value of the temperature gradient. The heat flux is plotted against the effective flux surface-averaged temperature gradient $\langle R/L_{T_e} \rangle = -R\ d\log(T,n)/d\rho_{tor} \langle |\nabla \rho_{tor}| \rangle$ which can be considered the effective normalized gradient driving the instabilities [9]. The different plasma shapes lead to a different value of $\langle |\nabla \rho_{tor}| \rangle$, which is larger when $\delta > 0$.
One immediately notes that the simulated powers for the experimental gradients are not radially constant, as would be expected under the assumption that all the input EC power is radially transported outwards across all flux surfaces between the radial location of power deposition ($\rho_{tor} = 0.4$ in this case) and the plasma edge. Also, and more importantly, the simulated transport levels are strongly overestimating the experimentally measured ones. This overestimation is particularly important in the core region (by a factor ~ 20 and ~ 40 for positive and negative δ respectively) and clearly not compatible with possible uncertainties in the input profiles. In agreement with [2], a radially dependent reduction of the heat transport when moving from positive to negative triangularity is found, however the results from the "*simple physics*" flux-tube model are obviously inadequate for modeling TCV discharges and a more accurate description is required.

5.2. "Full physics" model

The same series of runs as described in section 5.1 were repeated with the more comprehensive "*full physics*" model. In figure 9, the turbulent spectra for the experimental gradient cases are presented, showing the same radial dependence of different k_y modes contribution depending on δ as the ones described for the "*simple physics*" model. However we clearly see the reduction at negative δ for large ρ_{tor} values and not for $\rho_{tor} = 0.5$. The results obtained from the R/L_{T_e} scan are summarized in figure 10. With respect to the results obtained considering the "*simple physics*" model, there is a strong reduction of the electron heat flux $\langle Q_e \rangle$ when carrying out

the more realistic simulations. We studied the relative importance of every physical effect introduced with this more accurate model by switching on each term one after the other and monitoring the resulting variation of the heat flux. This exercise has been performed for the experimental conditions of the positive triangularity discharge at $\rho_{tor} = 0.5$ and $\rho_{tor} = 0.7$. For those two positions we also studied the effect of finite collisionality depending on δ.

Among the different effects that have been retained in this new series of runs, finite collisionality, because of its stabilizing role on TEMs [16], is the most important one. It contributes up to $\sim 60\%$ of the "*simple*" to "*full physics*" model reduction. As already shown in Ref. [2], its effect is strongest in the cases with $\delta_{\rm LCFS} < 0$ and is relatively more important as one moves from the core to the edge. Real electron to ion mass ratio and impurities, both contribute to further reducing heat transport. In particular, approximately 40% of the transport reduction is related to realistic m_D/m_e and another 10% to the impurities (this latter estimate is an average between the results at $\rho_{tor} = 0.5$ and 0.7). A minor effect is played by finite β effects, which in fact induce an *increase* in the heat flux by $\sim 10\%$. The actual electromagnetic contribution to transport related to magnetic field fluctuations is however negligible (less than a few percents of the total heat flux). Similarly low levels are found for the ion heat transport.

Despite the significant reduction of the electron heat transport going from "*simple*" to "*full physics*", a large overestimation of the simulated fluxes compared to the experimental ones, by at least a factor 6 (resp. 12), still remains for the core position (ρ_{tor}=0.5) of TCV plasma with positive (resp. negative) δ. Part of it might be explained by the high sensitivity of the heat transport to R/L_n as discussed below. On the other hand, at $\rho_{tor} = 0.95$ the simulated heat transport is in fact smaller than the measured one, an observation that we explain as a consequence of having artificially suppressed the

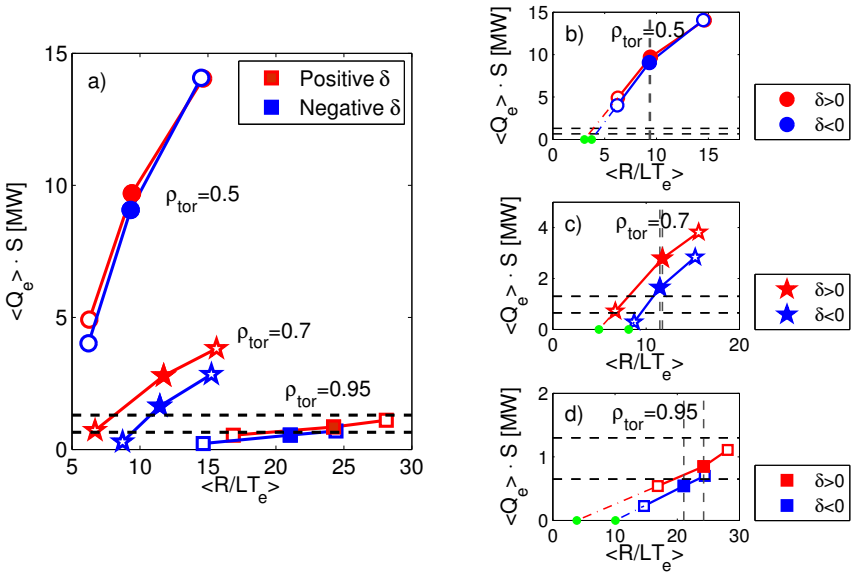

Figure 10. Same as figure 8 but for the "*full physics*" model results.

contribution of ETG turbulence there. Preliminary simulations limited to the electron gyroradius scales (not shown here) have been performed, showing that a non-negligible contribution to the transport is provided by ETG modes. These same simulations however also point out that the scale separation is probably not fully justified and a multi-scale approach is necessary towards the plasma edge.

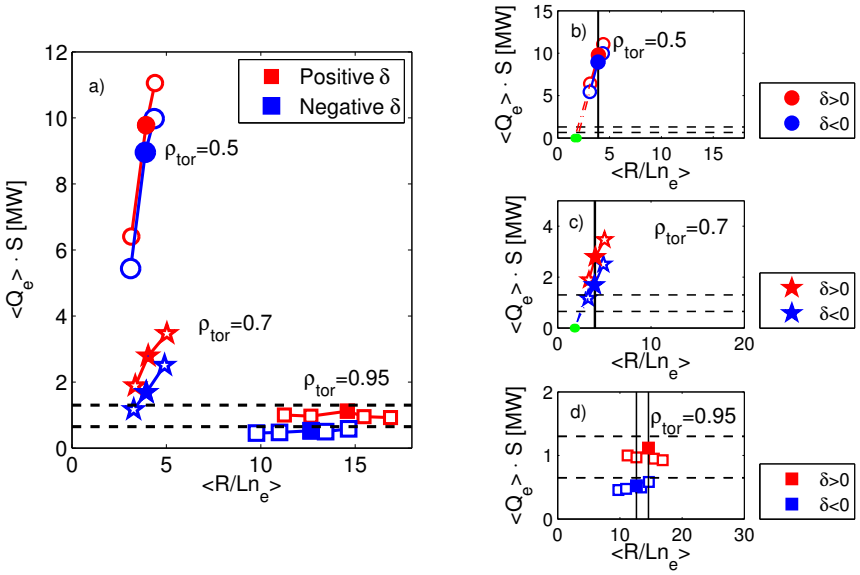

Figure 11. Same as figure 8 but using the "*full physics*" model set-up and scanning $\langle R/L_{n_e} \rangle$.

In order to complete the stiffness study, we scanned also the density gradient, upward and downward from the experimental value of temperature gradient. The results are shown in figure 11. At $\rho_{tor} = 0.95$ a $\pm 20\%$ variation of R/L_{n_e} does not change the heat transport level significantly as reflected in figure 11.*d* by curves which are non-stiff. At ρ_{tor} =0.5 and 0.7 instead, the sensitivity of the heat flux to a relative variation of the density gradient is stronger than the one to a variation of the temperature gradient as reflected by relatively stiff curves in figs. 11.*b*) and 11.*c*). Note that the aspect ratio of the axis of the subplots 10.(*b*) and 11.(*b*), as well as of subplots 10.(*c*) and 11.(*c*) and 10.(*d*) and 11.(*d*), has been kept, in order to allow the comparison between local stiffness with respect to a variation of R/L_{T_e} to stiffness with respect to a variation of R/L_n.

6. Discussion and conclusions

Linear and non-linear flux-tube gyrokinetic simulations using the GENE code have been performed in order to study (linear and non-linear) critical gradients and profile stiffness in the TCV tokamak and in particular their dependence on radius and triangularity. Experimental temperature and density profiles as well as magnetic geometry have been used, and for the considered discharges TEM and ETG modes have been identified as

the dominant instabilities. These modes not only have the largest growth rates at the ion and electron scales respectively but also provide the largest contribution to non-linear fluxes. ETG only provides a non-negligible contribution ($\sim 10\%$ of the measured heat flux) at the plasma edge ($\rho_{tor} = 0.95$).

Two types of non-linear simulations, corresponding to different levels of realism, have been carried out aiming at reproducing the experimental electron heat flux measurements and dependencies. Considering realistic m_D/m_e mass ratio, retaining finite collisionality, impurities and EM effects (without necessarily $B_\parallel$ fluctuations), was shown to be essential when simulating TCV conditions. Neglecting these effects and assuming $m_D/m_e = 400$, the simulated heat transport level is unrealistically high, overestimating the measurements by a factor ~ 20 in the core region and ~ 8 at the edge. A strong reduction is obtained with the "*full physics*" model. Finite collisionality is found to be responsible for most of the transport reduction, by a factor 2 at the core position. Realistic m_D/m_e leads to another $\sim 40\%$ reduction. The effects of impurities and finite β are of the same order and in opposite directions (C content reduces by $\sim 10\%$, while finite β increases the electrostatic heat flux, the contribution to the flux from electromagnetic fluctuations still being negligibly small).

Nonetheless, a non-negligible discrepancy between simulations and experiments persists. A significant overestimation of the heat transport level, by at least a factor 5, remains when simulating TCV core conditions, and it cannot be explained by uncertainties in the input values of the gradients, which are at most of the order of $\sim 20\%$. A better agreement is found for the edge simulations. For the outermost position considered ($\rho_{tor} = 0.95$), the simulations carried out at the ion scale, i.e. neglecting ETG contribution, are in fact underestimating the experimental electron heat flux. Our analysis however points out that a multiscale approach, resolving at the same time ion and electron scales, is required. Regarding the effect of negative triangularity, we do find a reduction by a factor $\sim$2 in the heat transport only for $\rho_{tor} \gtrsim 0.7$, in agreement with [2].

All these results show the intrinsic limit of flux-tube simulations applied to machines of similar size as TCV, where finite ρ^* effects are expected to be strong and need to be accounted for in the simulations in order to match experiments. It is already well established that the smaller $1/\rho^*$ the bigger the overestimation from flux-tube compared to global simulations [17, 18, 19]. If one considers just the radial profile of ρ_s, because of the decrease of temperature moving towards the LCFS, one can speculate that finite machine size stabilization is expected to be stronger in the plasma core with respect to the edge, i.e in agreement with our results. It is also known that for idealized cases one should in fact consider an effective $\rho^*_{\text{eff}} = \rho_s/\Delta_r$, accounting for gradient profile shapes [19] (Δ_r is the width of the gradient profile). How to correctly estimate Δ_r when dealing with experimental profiles (as well the dependence of finite ρ^* effects on all other plasma parameters) is still an open question that requires further dedicated investigations. Moreover, when transport is dominated by nonlocal effects, the concept of local profile stiffness as the local slope of the flux vs. normalized gradient curves is

not anymore well defined.

The only way to correctly account for finite $\rho^* = \rho_s/a$ effects is therefore performing global simulations. Such a study is underway and the results will be the subject of a follow-up paper. We remember that an attempt to infer semi-quantitative information regarding the stiffness properties of the profiles based one the flux tube simulations presented here was made in presenting the results obtained with the "*simple physics*" model in Ref. [4]. There, the simulated heat fluxes were all normalized such that for the experimental values of R/L_{T_e} the simulated heat fluxes were all of order unity and local slopes could be compared (see figure 14 in Ref. [4]). Such a speculative exercise was based on the assumption that finite ρ^* effects are independent from the plasma shape and the local value of gradients. We stress the fact that such an approach, and the results it leads to, has to be taken with extreme caution because any rescaling will inevitably change the local stiffness. This is particularly relevant at $\rho_{tor} = 0.5$ where there is almost no difference between positive and negative δ_{LCFS} flux-tube results. Furthermore, global effects are also expected to modify the value of critical gradients, potentially changing the overall picture. Therefore the question about profile stiffness still remains open and we cannot draw a clear and definitive conclusion about it. Nevertheless, keeping in mind our two initial hypotheses about the relation between profile stiffness, critical gradients and triangularity, if one looks at figure 10 it appears that the strongest effect exerted by negative triangularity is an increase of the critical gradient. This feature is in fact already visible with the "*simple physics*" model results (figure 8), however is less pronounced and one would also find negative critical gradients for the $\rho_{tor} = 0.95$ case. Considering the "*full physics*" results and linearly extrapolating (dot-dashed lines in figure 10), one finds that the critical temperature gradient is increased by a factor 2 (resp. 3) $\rho_{tor} = 0.7$ (resp. 0.95) going from $\delta_{\mathrm{LCFS}} > 0$ to $\delta_{\mathrm{LCFS}} < 0$. For the $\rho_{tor} = 0.5$ position there is still an upshift when going from positive to negative triangularity, but the relative difference is much smaller ($\sim 50\%$) and the overestimation of fluxes too large to be definitive. Nevertheless these results hint towards an upshift of $R/L_{T_e,crit}$ depending on δ. No significant effect of triangularity on local profile stiffness is found. however for both triangularities stiffness appears to be reduced as one moves towards the plasma edge. This is particularly evident when considering the dependence of the heat fluxes on the density gradient. Figure 11 shows that the heat fluxes are very sensitive to small variations of R/L_n at $\rho_{tor} = 0.5$ and 0.7, much less at $\rho_{tor} = 0.95$, where the profiles appear to be non-stiff, in agreement with the linear results shown in figures 4 and 5.

More work is clearly required to complete this study. Finite ρ^* effects are currently being investigated using the global version of GENE as well as a more accurate investigation of stiffness around the critical gradients is undergoing.

Acknowledgements

This project has received funding from the European Union's Horizon 2020 research and innovation programme under grant agreement number 633053. The views and opinions expressed herein do not necessarily reflect those of the European Commission. This work was supported in part by the Swiss National Science Foundation. The simulations have been carried out using the HELIOS supercomputer system at the Computational Simulation Centre of International Fusion Energy Research Centre (IFERC-CSC), Aomori, Japan, and on the Monte Rosa CRAY XE-6 platform of the Swiss National Supercomputing Center (CSCS).

References

[1] Camenen Y, Pochelon A, Behn R, Bottino A, Bortolon A, Coda S, Karpushov A, Sauter O, Zhuang G and the TCV team 2007 *Nuclear Fusion* **47** 510
[2] Marinoni A, Brunner S, Camenen Y, Coda S, Graves J P, Lapillonne X, Pochelon A, Sauter O and Villard L 2009 *Plasma Physics and Controlled Fusion* **51** 055016
[3] Kotschenreuther M, Rewoldt G and Tang W 1995 *Computer Physics Communications* **88** 128 – 140
[4] Sauter O, Brunner S, Kim D, Merlo G, Behn R, Camenen Y, Coda S, Duval B P, Federspiel L, Goodman T P, Karpushov A, Merle A and Team T 2014 *Physics of Plasmas* **21** 055906
[5] Villard L, McMillan B F, Sauter O, Hariri F, Dominski J, Merlo G, Brunner S and Tran T M Turbulence and zonal ow structures in the core and l-mode pedestal of tokamak plasmas submitted to *Journal of Physics: Conference Series*
[6] Jenko F, Dorland W, Kotschenreuther M and Rogers B N 2000 *Physics of Plasmas* **7**
[7] Hofmann F, Lister J B, Anton W, Barry S, Behn R, Bernel S, Besson G, Buhlmann F, Chavan R, Corboz M, Dutch M J, Duval B P, Fasel D, Favre A, Franke S, Heym A, Hirt A, Hollenstein C, Isoz P, Joye B, Llobet X, Magnin J C, Marletaz B, Marmillod P, Martin Y, Mayor J M, Moret J M, Nieswand C, Paris P J, Perez A, Pietrzyk Z A, Pitts R A, Pochelon A, Rage R, Sauter O, Tonetti G, Tran M Q, Troyon F, Ward D J and Weisen H 1994 *Plasma Physics and Controlled Fusion* **36** B277
[8] Camenen Y, Pochelon A, Bottino A, Coda S, Ryter F, Sauter O, Behn R, Goodman T P, Henderson M A, Karpushov A, Porte L and Zhuang G 2005 *Plasma Physics and Controlled Fusion* **47** 1971
[9] Angelino P, Garbet X, Villard L, Bottino A, Jolliet S, Ghendrih P, Grandgirard V, McMillan B F, Sarazin Y, Dif-Pradalier G and Tran T M 2009 *Phys. Rev. Lett.* **102**(19) 195002
[10] Lütjens H, Bondeson A and Sauter O 1996 *Computer Physics Communications* **97** 219 – 260
[11] Görler T, Lapillonne X, Brunner S, Dannert T, Jenko F, Merz F and Told D 2011 *Journal of Computational Physics* **230** 7053 – 7071
[12] Doerk H, Jenko F, Pueschel M J and Hatch D R 2011 *Phys. Rev. Lett.* **106**(15) 155003
[13] Jenko F and Dorland W 2002 *Phys. Rev. Lett.* **89**(22) 225001
[14] Pueschel M, Dannert T and Jenko F 2010 *Computer Physics Communications* **181** 1428 – 1437 ISSN 0010-4655
[15] Görler T 2009 *Multiscale effects in plasma microturbulence* Ph.D. thesis University of Ulm, Germany
[16] Vernay T 2013 *Collisions in Global Gyrokinetic Simulations of Tokamak Plasmas using the Delta-f Particle-In-Cell Approach: Neoclassical Physics and Turbulent Transport* Ph.D. thesis Ecole Polytechnique Fédérale de Lausanne (EPFL), Switzerland
[17] Lin Z, Ethier S, Hahm T S and Tang W M 2002 *Phys. Rev. Lett.* **88**(19) 195004
[18] Candy J, Waltz R E and Dorland W 2004 *Physics of Plasmas* **11**

[19] McMillan B F, Lapillonne X, Brunner S, Villard L, Jolliet S, Bottino A, Görler T and Jenko F 2010 *Phys. Rev. Lett.* **105**(15) 155001